

Comparison of microsphere deposition in porous media versus simple shear systems

Christina N. Brow^a, Xiqing Li^a, Jaro Rička^b, William P. Johnson^{a,*}

^a Department of Geology and Geophysics, University of Utah, Salt Lake City, UT, USA

^b Institute of Applied Physics, University of Bern, Bern, Switzerland

Received 11 May 2004; accepted 5 November 2004

Available online 15 December 2004

Abstract

Experiments were conducted to compare deposition fluxes of 1.1 and 5.7 μm carboxylate-modified polystyrene latex microspheres in packed porous media and simple shear systems. A range of flow conditions were examined in the packed columns (2, 4, and 8 m day^{-1} average pore water velocities), and impinging jet cells (0.01, 0.03, and 0.05 ml min^{-1} jet discharge rates), and were scaled to yield equivalent near-surface velocities in the two systems. Two ionic strengths (0.006 and 0.02 M NaCl) were examined under electrostatically unfavorable attachment conditions, whereas electrostatically favorable conditions were examined at a single ionic strength (0.02 M). Deposition fluxes onto quartz and glass substrata were examined. Initial attachment fluxes were sometimes higher, sometimes lower, in the porous media relative to the simple shear systems under equivalent conditions. Deposition efficiencies (deposition flux normalized to deposition flux under favorable conditions) were consistently higher in the porous media relative to the impinging jet when the angular substrate (quartz) was examined, whereas deposition efficiency was lower in the glass bead porous media relative to the glass substratum in the impinging jet under the one condition examined. These results corroborate the hypothesis that deposition in quartz media is enhanced by the presence of rear stagnation points, whereas this phenomenon was not manifested in the smooth spherical porous media. Hydrodynamic drag was implicated as an important governor of the initial attachment flux on the basis of lack of deposition of 5.7 μm microspheres despite theoretical predictions, as well as an observed lack of increase in 1.1 μm microsphere attachment flux with increased flow rate under favorable conditions, and an observed decrease in 1.1 μm microsphere attachment flux with increased flow rate under unfavorable conditions. Experiments run with a mixture of the 1.1 and 5.7 μm microspheres indicated association of the different sized microspheres on the surface. Results from the packed porous media suggested indirect association (via the hydrodynamic field) at the grain surface, whereas observations in the impinging jet indicated direct association of the 1.1 and 5.7 μm microspheres.

© 2004 Elsevier B.V. All rights reserved.

Keywords: Colloid transport; Attachment flux; Hydrodynamic drag; Rear stagnation points; Microspheres

1. Introduction

The potential role of hydrodynamic drag in preventing colloid attachment has received far less attention than colloid–surface interactions in studies examining the transport of colloids in groundwater. In natural systems, e.g. subsurface sediments, electrostatic colloid–surface interaction forces are dominantly unfavorable (all surfaces are domi-

nantly negatively charged) [1,2]. The role of colloid–surface interaction forces on the removal rate of colloids under unfavorable conditions has been well investigated, although not completely understood, in both porous media [3,4] and simple shear systems (e.g. parallel plate and impinging jet) [5,6]. These experiments show that colloid removal rates from solution are in qualitative agreement with theory; that is, increased ionic strength leads to greater removal rates. However, quantitative disagreements between theory and experiment are paramount, the most important being that in experiments removal occurs under unfavorable conditions. Removal from

* Corresponding author. Tel.: +1 801 581 5033; fax: +1 801 581 7065.

E-mail address: wjohnson@mines.utah.edu (W.P. Johnson).

solution under unfavorable conditions has been attributed variously to nanoscale surface charge heterogeneity [7,8], surface roughness [7,9,10], tethering by surface polymers [11,12], and lack of accounting for other non-DLVO forces such as Lewis acid–base forces [10], among several non-DLVO potential contributors to interaction forces.

Very recent experiments comparing deposition fluxes of bacteria in impinging jet versus packed column systems attributed a majority of deposition under the unfavorable conditions to deposition in secondary energy minima [13,14]. These experiments indicated that deposition efficiencies were much greater in the packed column relative to the impinging jet, whereas the majority of bacteria retained in the packed columns were eluted by introduction of pure water, suggesting that these bacteria had been deposited in secondary energy minima that were eliminated by the reduction in solution ionic strength. Association with surfaces via the secondary energy minimum would subject bacteria to translation along the porous media surface via fluid drag, suggesting that deposition within the porous media occurred in rear stagnation points in the near surface flow field.

Investigators have been primarily interested in hydrodynamic drag in so far as it influences the subsequent attachment of particles at the surface downstream from an attached particle [5,15–17]. Under many environmental conditions, attached colloids can block the subsequent attachment of mobile colloids [18,19]. The excluded area associated with an attached colloid under blocking conditions arises partly from electrostatic repulsion between the attached and mobile colloids [20], and this component of the excluded area is inversely related to solution ionic strength [18–20]. The excluded area associated with an attached colloid is also directly related to the pore water velocity, a “shadow” effect arising from asymmetric extension of the excluded area leeward of the attached colloid as the fluid velocity increases [21]. This effect has been observed in simple shear systems [22–25] as well as in porous media [21].

Researchers have also been interested in the detachment of particles, but hydrodynamic forces driving detachment have typically been considered dominantly in the form of hydrodynamic collisions between mobile and attached particles [26–28]. The lack of focus on potential direct effects of hydrodynamic drag may result from the majority of colloid transport studies examining sub- μm sized particles, for which hydrodynamic drag may indeed be negligible. However, for colloids of sizes $1\ \mu\text{m}$ and larger, hydrodynamic drag may influence the ability of these colloids to attach to surfaces exposed to fluid advection.

This paper describes experiments performed to compare the transport behavior of 1.1 and $5.7\ \mu\text{m}$ carboxylate modified latex microspheres in packed porous media and simple shear systems in order to qualitatively elucidate the effect of hydrodynamic drag on attachment rates. It also describes experiments performed to examine possible direct or indirect association of 1.1 and $5.7\ \mu\text{m}$ microspheres within the hydrodynamic field at the grain surface.

2. Materials and methods

2.1. Materials

Spherical fluorescent carboxylate-modified polystyrene latex microspheres of two sizes (diameters of 1.1 and $5.7\ \mu\text{m}$) were used in all experiments except as noted. The $1.1\ \mu\text{m}$ microsphere stock suspension (Molecular Probes, Inc., Eugene, OR) particle concentration was $2.7 \times 10^{10}\ \text{ml}^{-1}$, with a NaN_3 concentration of $2\ \text{mM}$. The $5.7\ \mu\text{m}$ microsphere stock suspension (Bangs laboratories, Inc., Fishers, IN) particle concentration was $9.4 \times 10^7\ \text{ml}^{-1}$, with 0.01% of Tween-20, and $2\ \text{mM}$ of NaN_3 . Stock solutions were diluted in NaCl solution at the desired strength (0.006 and $0.02\ \text{M}$). MOPS buffer ($2.2\ \text{mM}$) was also present in a subset of the experiments as described below. Influent solution pH in buffered and unbuffered systems was 7.0 and 6.0 , respectively.

Column and impinging jet experiments were intended to be comparable. Fluxes in both systems were determined under favorable and unfavorable conditions. Furthermore, fluxes in both systems were determined for both 1.1 and $5.7\ \mu\text{m}$ microspheres under both solo and mixed conditions, however, the mixed conditions were examined only under unfavorable conditions.

Favorable conditions were generated differently in the column versus the impinging jet system. In the impinging jet system, favorable conditions were generated by coating the substratum with polyethylenimine (PEI, Sigma-Aldrich, St. Louis, MO), and only the $1.1\ \mu\text{m}$ microspheres were examined in these experiments. The coating procedure involved soaking the substratum overnight in $0.118\ \text{g}$ PEI per $100\ \text{ml}$ deionized water. The influent particle concentration was $1.35 \times 10^7\ \text{ml}^{-1}$, and ionic strength was $0.02\ \text{M}$ with no buffer.

In the column system, favorable conditions were generated by examining the transport of $0.93\ \mu\text{m}$ amine-functionalized polystyrene latex microspheres (Molecular Probes, Inc., Eugene, OR), since PEI equilibration of the substrata was problematic for the relatively large quantities of sediment used in the packed column experiments. The amine-functionalized microspheres had a stock concentration of $4.5 \times 10^{10}\ \text{ml}^{-1}$, and a surface charge of $0.9176\ \text{mequiv. g}^{-1}$. MOPS buffer ($2.2\ \text{mM}$) was used, and the ionic strength was $0.001\ \text{M}$. Presence or absence of buffer and changes in ionic strength were expected to insignificantly effect attachment under favorable conditions, hence, attachment fluxes under favorable conditions in the packed column and impinging jet systems were contrasted despite their different buffer and ionic strength conditions.

Column experiments under favorable conditions examined attachment on both quartz and glass-packed media, since angularity of the grains contrasts strongly between those two substrata. Impinging jet experiments under favorable conditions examined quartz only, since the flat PEI-coated quartz substratum was assumed to be equally representative of favorable attachment conditions for glass and quartz.

The majority of experiments concerned unfavorable conditions. Due to limited availability of the 1.1 μm microsphere stock used in the experiments, influent concentrations in the packed column experiments under unfavorable conditions were decreased to $3.38 \times 10^6 \text{ ml}^{-1}$, whereas influent concentrations in the impinging jet experiments were $1.35 \times 10^7 \text{ ml}^{-1}$. The resulting fluxes ($\text{mm}^{-2} \text{ day}^{-1}$) were normalized by influent concentration (mm day^{-1}) to account for these concentration differences. MOPS buffer (2.2 mM) was used in both systems for both substrata with the exception of the impinging jet for the quartz substratum, since quartz-solution interaction would not be expected to yield significant changes in solution chemistry.

A portion of the experiments run in both the jet and column systems examined transport of a mixture of the 1.1 μm microspheres and 5.7 μm microspheres (1.35×10^7 and $9.4 \times 10^5 \text{ ml}^{-1}$ for the 1.1 and 5.7 μm microspheres, respectively) in order to examine possible direct or indirect influence of attachment of one on the other. These experiments were performed under unfavorable conditions, and no buffer was used.

2.2. Impinging jet experiments

Total internal reflection fluorescence, TIRF, was used to examine attachment of microspheres in the impinging jet. TIRF exploits the evanescent wave at a solid–liquid interface [29]. Because the depth of the evanescent field is limited to a short distance from the interface (typically $<200 \text{ nm}$), TIRF offers a means to excite only those particles at, or very near the solution–substratum interface. For the purpose of quantifying attachment and detachment of particles at the interface, this method is superior to systems using bulk fluorescence, where it is difficult to distinguish between attached particles and particles in the bulk fluid [29].

An evanescent wave was developed at the substratum–liquid interface with a Lexel Model 85 argon laser (Lexel Corporation, Palo Alto, CA) tuned to a wavelength of 488 nm. The laser was mounted on a rotating arm with its rotational axis centered on the center of the flow cell above the objective on the microscope stage. The microscope was an Axiovert 35 inverted microscope (Zeiss, Oberkochen, West Germany). Bandpass filters were used to block scattered light. A $10\times$ long-distance working objective (Zeiss, Oberkochen, West Germany) was used to magnify the image.

A Kappa CF8/DX CCD camera (Kappa, Gleichen, Germany) was used to collect images at regular intervals. The black and white images of 8-bit digitalization depth had an array size of 752×582 pixels, with a corresponding area of 0.187 mm^2 . The setup was equipped with a synchronized shutter (Vincent Associates, Rochester, NY, Model VS14S1T0) to block light except during image acquisition, in order to avoid photo bleaching of microspheres.

The coordinates of attached microspheres in the images were determined by a modified version of the FIND routine from the IDL-astro library (<http://idlastro.gsfc.nasa.gov/>

[ftp/pro/idlphot/](http://ftp.pro.idlphot/)). The FIND routine filtered out noise by selecting a background pixel value, and then detected particles based on luminosity peaks above a selected threshold. The coordinates of the particle corresponded to the centroid of the luminosity peak.

Data produced was in the form of a net attached population for each time step recorded, as well as the arrival and departure times of the particles. Singulars, particles that appeared in only one image, were eliminated in the analysis as they could represent either random noise or particles whose paths brought them into the evanescent field though they did not attach to the substratum. Detachment events were recorded when the particle luminosity decreased below a specified threshold. A more detailed description of the software can be found in Lüthi and Rička [30].

Both quartz and borosilicate glass substrates were used in the impinging jet flow cell. Quartz substrates were re-used, whereas a new glass substrate was used for each experiment. The cleaning procedures were the same for both quartz and glass substrata. Substrata were washed with 2% Deconex (Borer Chemie AG, Zuchwil, Switzerland) and rinsed with deionized water. They were then sonicated in chromic acid for 15 min, rinsed with deionized water, and sonicated in 1 M HCl for 15 min after which they were rinsed with ultra pure water (Millipore Corp. Bedford, MA), and dried with N_2 gas.

The diameter of the impinging jet used was $500 \mu\text{m}$. The distance from the jet outlet to the impinging surface was $650 \mu\text{m}$. Additionally some qualitative observations were made using a parallel plate flow cell. Particles were injected into the flow cell using a syringe pump (KD Scientific, Holliston, MA). Particle injection duration was 180 min, followed by elution with particle-free solution. Flow rates in the impinging jet flow cell were designed to correspond to pore water velocities in the column and were varied ($0.01, 0.03, 0.05 \text{ ml min}^{-1}$). Particle attachment flux ($\text{mm}^{-2} \text{ day}^{-1}$) was determined by dividing the net attachment rate by the area of the substrate imaged and was normalized to influent particle concentration (mm day^{-1}).

The particle transport model described in Yang et al. [31] was used to develop DLVO interaction forces curves and predict attachment fluxes for the experimental conditions used in the impinging jet system. The model takes into account convection, Brownian diffusion, hydrodynamic interactions, and gravity, as well as van der Waals and electrostatic double layer surface force interactions. The electrostatic double layer surface force interactions were calculated using the approximate HHH expression assuming constant potentials [32]. Input parameters for the particle transport model included the jet radius, the distance from the jet outlet to the impinging surface, particle radius, ionic strength of the solution, Reynolds number, fluid intensity, Hamaker constant, and the surface potentials of the particles and the substratum.

In the particle transport model, a single parameter (the fluid intensity) was used to describe the axial and radial velocities in the impinging jet system based on axial and radial coordinates. The fluid intensity was determined by numerical

fitting of solutions of the stream function–vorticity (simplified Navier–Stokes) equations as described in Yang et al. [31]. The combined Hamaker constants for the polystyrene microsphere–water–substratum systems were estimated from the Hamaker constants of the individual materials:

$$A_{132} = \left(\sqrt{A_{11}} - \sqrt{A_{33}} \right) \left(\sqrt{A_{22}} - \sqrt{A_{33}} \right) \quad (1)$$

A_{11} and A_{33} are the Hamaker constants for polystyrene and water and are given by Israelachvili [33] as 6.60×10^{-20} and 3.70×10^{-20} J, respectively. A_{22} is the Hamaker constant of the substrate and is given as 8.86×10^{-20} J for quartz [34] and 6.34×10^{-20} J for glass [35]. The resulting combined Hamaker constants for the quartz and glass systems were 6.8×10^{-21} and 3.84×10^{-21} J, respectively.

Zeta potentials were used to represent the surface potentials in the particle transport model. Zeta potentials for the polystyrene microspheres were derived from measured electrophoretic mobilities (ZetaPALS, Brookhaven Instruments Corporation, Holtsville, NY) using the von Smoluchowski equation [36], as well as soft particle electrophoresis theory developed by Oshima [37,38], which assumes a charge distribution in an ion-penetrable surface layer of finite thickness. Various workers have applied this theory to electrophoretic mobilities of microbial colloids [39,40]. Over the ionic strength range from 0.006 to 0.02 M, the surface potentials for the 1.1 μm polystyrene microspheres ranged from -65.1 to -63.6 mV and -24.9 to -9.25 mV based on conventional and soft particle electrophoresis approaches, respectively. The zeta potential for the quartz substrate was estimated from values given in Elimelech et al. [41] (-50 and -30 mV for 0.006 and 0.02 M ionic strengths, respectively). The zeta potential of the glass substrate (-32.0 mV over the ionic strength range examined here) was given by Bergendahl and Grasso [35]. The particle transport model was insensitive to the surface potential of the collector under favorable conditions ($+10$ to $+30$ mV). Therefore, in particle transport simulations, a value of $+20$ mV was used to represent the surface potential of the PEI-coated quartz substratum.

2.3. Packed column experiments

Column experiments using packed porous media were used to examine the transport of polystyrene microspheres for a range of ionic strengths (0.006–0.02 M). Spherical glass beads (Cataphote Inc., Jackson, MS) and quartz sand (Unimin Corp., New Canaan, CT) were used as the porous media in cylindrical plexiglass columns 20 cm in length and 3.81 cm in diameter. The cleaning procedure for the glass beads was based on that by Bergendahl and Grasso [35]. The beads were sequentially rinsed with acetone and hexane and then soaked in concentrated HCl for about 12 h. After repeated rinsing with deionized water, the glass beads were then soaked in 0.1 M NaOH for about 12 h followed by repeated rinsing in ultra pure water until the conductivity was less than 20 μmho (Conductance/TDS Model 72, Engineered Systems and De-

sign, Newark, DE). The cleaning procedure for the quartz sand involved soaking for 24 h in concentrated HCl, thorough rinsing in either deionized water or Milli-Q, and baking at 850 °C overnight. The dried quartz sand was preserved under vacuum (packed into a sterile dry bottle filled with N_2 gas) and stored in a dry place until needed. The quartz sand was rehydrated just before use by boiling it in Milli-Q for 1 h, and drying overnight at 100 °C.

The media was dry-packed by adding the media in small increments and using mild vibration. The columns were purged with CO_2 (a soluble gas) for at least 30 min to remove air, and were pre-equilibrated by a salt solution of the desired ionic strength for six pore volumes. After pre-equilibration, three pore volumes of the microsphere suspension were injected into the column followed by a seven pore volume elution with the salt solution. Flow rates in the column were varied to achieve three average pore water velocities (2, 4, and 8 m day^{-1}). Not all conditions in the matrix resulting from two ionic strength and three flow rate variations were examined in the packed column. Rather, a sufficient subset to allow comparison to the impinging jet was examined. Column effluent samples were collected and analyzed via flow cytometry (BD FACScan, Becton Dickinson and Co., Franklin Lakes, NJ). A more detailed description of the column experiments can be found in Li et al. [42].

An advection–dispersion model with rate constants to describe colloid removal from solution (FlowTrak2.2) [43] was used to characterize column experiment results. A detailed description of this model can be found in Li et al. [42]. Fluxes from solution to the sediment (normalized to influent concentration) (mm day^{-1}) were determined for the column experiments by converting the experimental removal rate, k_f (h^{-1}) to deposition flux (j_{dep}) as follows:

$$j_{\text{dep}} = 24k_f \frac{\theta}{(1-\theta)} \frac{r}{3} \quad (2)$$

where the leading factor (24) converts days to hours, and θ is the porosity of the packed media. The term involving porosity converts the flux from per volume of solution to per volume of sediment. The term $r/3$ represents the ratio of the volume ($(4/3)\pi r^3$) to surface area ($4\pi r^2$) of sediment grains. Sediment grains were assumed to be spherical with a diameter of 510 μm . For the glass beads, a distribution of removal rates was used to simulate the data [42], and in this case the mean removal rate was used to determine attachment flux.

For both column and impinging jet experiments, the attachment flux ($\text{mm}^{-2} \text{day}^{-1}$) was normalized to the influent particle concentration (mm^{-3}) to yield a normalized flux (mm day^{-1}). Deposition efficiencies were calculated by dividing the attachment flux for a given ionic strength and flow condition by the flux for the corresponding flow rate under favorable attachment conditions.

Fluid flow models were used to estimate fluid velocities at the center of colloids attached to the surface in both systems. In the packed columns, the pore domain was represented by a constricted tube model [44]. The fluid velocity (e.g. m s^{-1})

at the centerpoint of an attached colloid anywhere along the idealized pore can be calculated as follows:

$$v_{\text{fluid}} = 2 \frac{Q/N_{\text{pore}}}{(\pi/4)d_z^2} \left[1 - \left(\frac{d_z/2 - a_{\text{colloid}}}{d_z/2} \right)^2 \right] \quad (3)$$

where a_{colloid} is the radius of the colloid, Q the volumetric flow rate, and

$$N_{\text{pore}} = \frac{A_{\text{column}}\theta}{(\pi/4)d_{\text{effective}}^2} \quad (4)$$

and

$$d_z = 2 \left\{ \frac{d_c}{2} - \left[4 \left(\frac{d_c}{2} - \frac{d_{\text{max}}}{2} \right) \left(0.5 - \frac{z}{h} \right)^2 \right] \right\} \quad (5)$$

where A_{column} is the cross-sectional area of the column, θ the porosity of the packed media, and $d_{\text{effective}}$ and d_{max} are determined as follows [45]:

$$d_{\text{effective}} = \frac{d_c}{0.470} \quad (6)$$

d_c is the average diameter of pore constrictions [45]:

$$d_c = \frac{d_g}{2.5658} \quad (7)$$

d_g is the average diameter of packed media grains, d_{max} the maximum pore diameter [46]:

$$d_{\text{max}} = 2.141d_c \quad (8)$$

z is the length along the pore and h the pore length (set equal to the pore diameter).

The formula given above for d_z (Eq. (5)) differs from that given by Bergendahl and Grasso [44] in that the first d_c term above was substituted for d_{max} in the formula presented [44]. As well, the first minus sign in the above formula replaces a plus sign in the formula presented [44]. Although both equations are reasonable, these modifications were made in order to conform to a pore domain as shown in inset a of Fig. 1, whereas the formula presented by Bergendahl and Grasso [44] conforms to the pore domain in inset b of Fig. 1 despite contrary schematics in their paper.

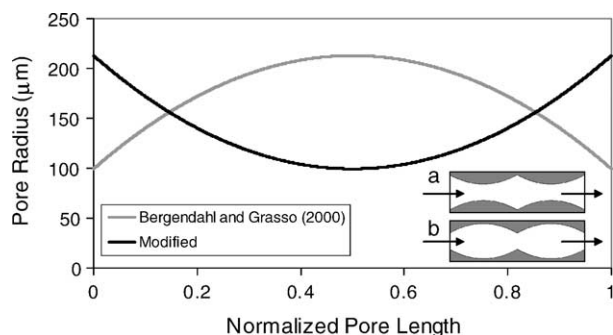


Fig. 1. Pore geometry calculated from Eq. (3) vs. those calculated from the corresponding equation in Bergendahl and Grasso [44]. Insets a and b show connected pore throats for the two pore domains calculated by the two different equations.

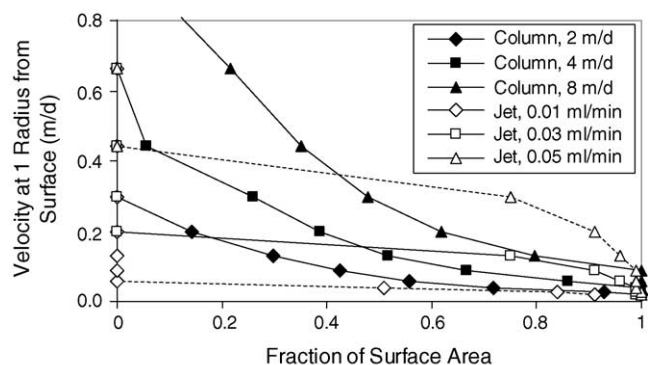


Fig. 2. Cumulative velocity distributions. Symbols represent cumulative velocity distributions at one radius distance from the grain surface ($0.55 \mu\text{m}$). The cumulative velocity distributions were estimated for the packed column (closed symbols) and for the area of observation above the impinging jet (open symbols). For the column, the velocities represent those expected within an idealized pore domain based on constricted tube geometry [42]. For the jet, the velocities were determined by fitting solutions of the Navier–Stokes equations to stagnation flow patterns as given Dabros and van de Ven [5]. Though the distribution of velocities is greater in the column, the averages are similar to those from the impinging jet. Lines do not represent data, but rather are present only to clarify trends.

Fig. 2 shows the cumulative velocity distributions at one radius distance from the surface ($0.55 \mu\text{m}$) for both the sediment column (closed symbols) and the area of observation in the impinging jet (open symbols). For the column, the fluid velocities represent those expected within an idealized pore domain based on constricted tube geometry as described above. For the impinging jet, the fluid velocities were determined by numerical solution of the Navier–Stokes equations as described above. Note that hydrodynamic drag scales directly to fluid velocity and colloid diameter; hence, comparison of velocities between the impinging jet and the column also yields comparison of hydrodynamic drag between the two systems. The cumulative velocity profiles for the column probably overestimate the low values in the velocity distribution, since the constricted tube model does not account for rear stagnation points. As determined from the cumulative velocity histograms (Fig. 2), the flow rates corresponding to 2, 4, and 8 m day^{-1} average pore water velocities in the column best corresponded to the 0.01, 0.03, and 0.05 ml min^{-1} flow rates, respectively, in the impinging jet. The distribution of velocities was greater in the column relative to the jet (Fig. 2), whereas the average value of the velocity was qualitatively similar between the two systems when the corresponding flow rates were compared (low, intermediate and high for each system, respectively).

3. Results

3.1. Example results

Fig. 3 shows example net attachment curves at 0.006 M ionic strength for all three flow rates. The duration of particle

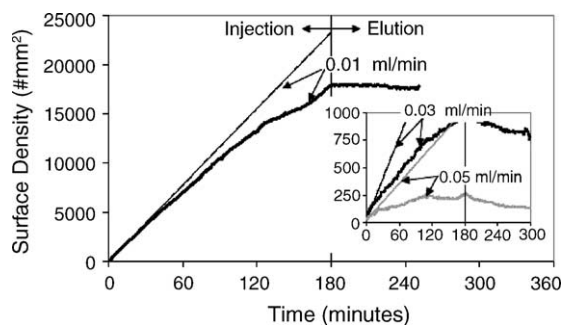


Fig. 3. Representative net attachment curves at 0.006 M ionic strength in the impinging jet for all three flow rates. Duration of injection of microspheres was 180 min, which was followed by elution with microsphere-free solution. The slope of the injection portion of each curve yields the attachment flux ($\text{mm}^{-2} \text{min}^{-1}$). The inset shows details for the 0.03 and 0.05 ml min^{-1} flow rates. Also shown are the trend lines for the first 10 min of the particle injection. The observed decrease in number density during elution was due to detachment rather than photobleaching of the microspheres.

injection was 180 min, followed by elution with particle-free solution. The slope of the curve yields the attachment flux ($\text{mm}^{-2} \text{min}^{-1}$). Also shown are the trend lines for the first 10 min of the particle injection. Trend lines do not go through zero, since experiments started with some small number of attached microspheres. The inset shows details for the 0.03 and 0.05 ml min^{-1} flow rates. Note that the observed decrease in attached number density during elution was due to detachment, and was not due to photobleaching of the microspheres. Absolute numbers of detachment events were too low to make statistically significant comparisons of detachment for the different experimental conditions. The trend lines shown in Fig. 3 represent attachment flux determined from the first 10 min of the particle injection and this initial flux decreased with increased flow rate (normalized fluxes of 12.28, 1.34, and 0.37 mm day^{-1} for 0.01, 0.03, 0.05 ml min^{-1} , respectively). Attachment flux also decreased with increasing experiment time (diverged from initial slope) for all three flow rates (Fig. 3) indicative of blocking by attached microspheres, although determination of the excluded area under unfavorable conditions is complicated by the presence of a limited number of attachment sites [47]. The increased deviation from the trend lines with increased flow rate indicates a hydrodynamic component to the excluded area associated with attached microspheres (shadow effect), as observed by others [5,15–17]. Blocking was also observed under favorable conditions but to a much lesser degree than under unfavorable conditions, as expected from the surface being predominantly favorable for attachment.

Fig. 4 depicts a typical breakthrough–elution curve for 1.1 μm microspheres in the column system in the presence (mixed, closed symbols) versus the absence (solo, open symbols) of the 5.7 μm microspheres. The effect of mixing the microspheres will be discussed in a separate section. In Fig. 4, C_0 and C are the injected and effluent particle concentrations, respectively. The duration of particle injection was ≈ 3.5 h and was followed by ≈ 8 h of elution with particle-free solu-

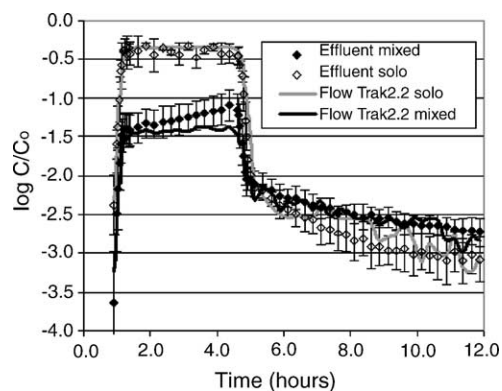


Fig. 4. Breakthrough–elution curves for 1.1 μm microspheres in the packed column in the presence (mixed, closed symbols) and absence (solo, open symbols) of 5.7 μm microspheres. Pore water velocity was 4 m day^{-1} , ionic strength was 0.02 M. C_0 and C represent the injected and eluted concentrations, respectively. The duration of the particle injection was ≈ 3.3 h and was followed by ≈ 8 h of elution with particle-free solution. Error bars represent standard deviations in results from replicate experiments ($n=4-7$). Lines represent simulations using Flow Trak 2.2 [41], a particle tracking model for porous media that includes an attachment rate distribution for the injected microsphere population.

tion. Error bars represent standard deviations in results from replicate experiments ($n=4-7$). Note that lines without symbols represent simulations by the kinetic model, which provided kinetic constants used to determine the removal fluxes. The flat breakthrough plateaus (e.g. Fig. 4) indicate an absence of temporal decreases in attachment flux (blocking) in the column experiments. Hence, the removal rates were constant throughout the duration of the column experiments, except where noted. The persistent low concentrations of microspheres following breakthrough of the injected pulse indicate slow re-entrainment of microspheres.

3.2. Attachment flux in the impinging jet

Initial attachment fluxes under unfavorable conditions in the impinging jet system increased with increasing ionic strength at all flow rates for both the quartz and glass substrata, with the exception of the low flow rate for quartz. At the low flow rate, initial attachment fluxes to quartz were insensitive to ionic strength (Fig. 5, Table 1).

Initial attachment fluxes under unfavorable conditions were similar, but slightly higher, for glass relative to quartz at the high flow rate (Fig. 5, Table 1). The attachment fluxes decreased with increased flow rate for both the quartz and glass substrata at all ionic strengths. However, as flow rate decreased, the fluxes to quartz increased dramatically relative to glass, especially at the low ionic strength.

Initial attachment fluxes to PEI-coated quartz (favorable conditions) were virtually identical for all three flow rates (isolated open symbols in Fig. 5, Table 1), and were similar to the initial attachment fluxes achieved at the low flow rate under unfavorable conditions on the quartz substratum (Fig. 5, Table 1). This similarity suggests that at the

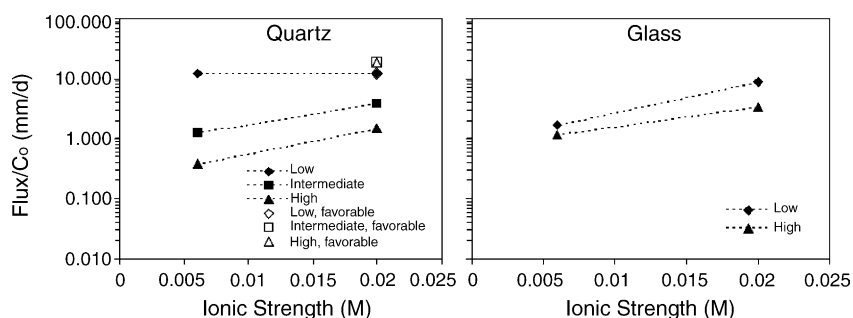


Fig. 5. Initial attachment flux (mm day^{-1}) vs. ionic strength for $1.1 \mu\text{m}$ microspheres in the impinging jet system with both quartz and glass substrates. Isolated open symbols represent experimentally determined initial attachment fluxes onto PEI-coated quartz at 0.02 M ionic strength for each of the three flow rates. Lines do not represent data, but are present only to clarify trends.

Table 1

Initial flux in mm day^{-1} in the impinging jet under unfavorable and favorable conditions for both quartz and glass substrata

Flow rate (ml min^{-1})	Substrata	0.006 M ionic strength		0.02 M ionic strength		
		Unfavorable	Favorable	Unfavorable	Favorable	
					Experimental	Model
0.01	Quartz	12.28		12.19	12.38	7.50
0.03	Quartz	1.27		3.89	18.41	8.87
0.05	Quartz	0.37		1.50	18.07	11.06
0.01	Glass	1.67		8.82		
0.05	Glass	1.13		3.43		

Initial flux under favorable conditions was determined only for the 0.02 M ionic strength on quartz. Differences in ionic strength would insignificantly affect flux under favorable conditions based on simulations by the particle transport model. It was also assumed that the flat, PEI-coated substratum was equally representative of quartz and glass. Also shown are the model-predicted fluxes to quartz under favorable conditions at the 0.02 M ionic strength.

low flow rate, there was no effective barrier to attachment to quartz. In contrast, the initial attachment fluxes to glass showed sensitivity to ionic strength at the low flow rate (Fig. 5, Table 1).

The particle transport model predicted negligible flux to the surface under all unfavorable conditions. The corresponding DLVO–force plots are shown in Fig. 6. The plots shown

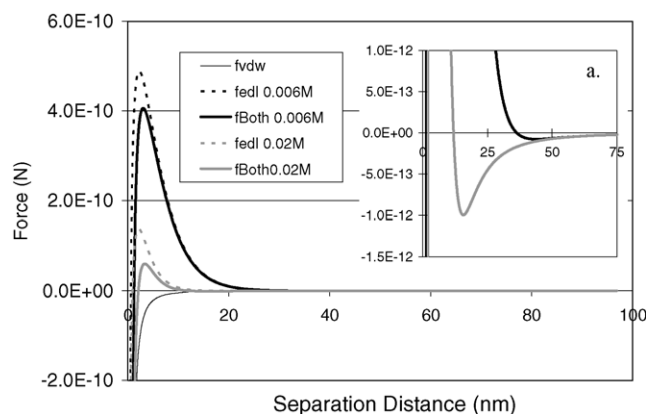


Fig. 6. DLVO force plots for 0.006 and 0.02 M ionic strengths for $1.1 \mu\text{m}$ microspheres, calculated by the particle transport model of Yang et al. [29] using zeta potentials from soft particle electrostatic theory. In the legend, “fvdw” is the van der Waals interaction force, “fedl” is the electrostatic double layer interaction force, and “fBoth” is the sum of “fvdw” and “fedl”. Inset shows slight attractive forces ($< \text{pN}$) associated with secondary minima. Force plots using ion-impenetrable sphere (hard sphere) assumptions were similar (not shown) except that the repulsive barriers were higher.

were developed using soft particle surface potentials. Force plots developed using hard particle zeta potentials were similar, except that they yielded greater barriers to attachment. The inset reveals slight attractive forces ($< \text{pN}$) associated with secondary minima. The observation of attachment in experiments in spite of theoretical predictions is a well-known phenomenon that was briefly described in Section 1, however, determination of the specific mechanism falls outside the scope of this paper.

Model-predicted attachment fluxes under favorable conditions matched experimentally determined attachment fluxes under favorable conditions (PEI-coated quartz). Model-predicted attachment fluxes were $7.5, 8.9,$ and 11.1 mm day^{-1} versus experimentally determined fluxes of $12.4, 18.4,$ and 18.1 mm day^{-1} , at $0.01, 0.03,$ and 0.05 ml min^{-1} , respectively (Table 1). This match indicates that the model captured the essential processes governing transport and attachment under favorable attachment conditions.

3.3. Attachment flux in the packed column

The trends in initial attachment flux versus ionic strength and flow rate under unfavorable conditions in the packed column were qualitatively equivalent to those in the impinging jet (Fig. 7, Table 2). However, unlike the impinging jet, the effect of a repulsive barrier to attachment was evident for both substrata at all flow rates, since the initial fluxes under favorable conditions (isolated open symbols)

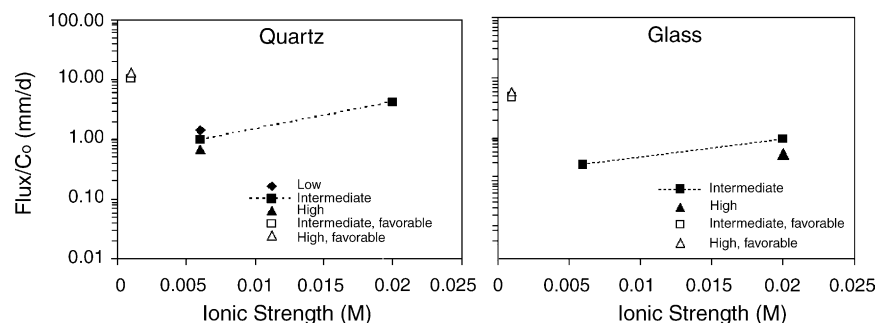


Fig. 7. Initial attachment flux vs. ionic strength and flow rate for 1.1 μm microspheres in the column, with both quartz and glass substrata. Isolated open symbols represent experimentally determined attachment fluxes under favorable conditions (amine-functionalized microspheres, 0.001 M) at the intermediate and high flow rates. Lines do not represent data, but are present only to clarify trends.

Table 2

Flux in mm day^{-1} in the packed column under unfavorable and favorable conditions for both quartz and glass substrata

Flow rate (m day^{-1})	Substrata	0.006 M ionic strength		0.02 M ionic strength	
		Unfavorable	Favorable ^a	Unfavorable	Favorable
2.0	Quartz	1.40			
4.0	Quartz	0.99	10.18	4.10	
8.0	Quartz	0.68	13.2		
2.0	Glass				
4.0	Glass	0.37	4.8	0.97	
8.0	Glass		6.0	0.55	

^a Flux values under favorable conditions for both quartz and glass were determined at an ionic strength of 0.001 M, but were listed in the table under the 0.006 M ionic strength to condense the table. Differences in ionic strength would insignificantly affect flux under favorable conditions based on simulations by the particle tracking model. Flux under favorable conditions was determined from separate experiments for the quartz and glass substrata, since in the packed column the angularity of the grains contrasted strongly between those substrata. Experiments performed at the low flow rate in glass porous media showed filter ripening, precluding determination of an initial attachment rate.

were significantly greater than those under unfavorable conditions (Fig. 7, Table 2). As was observed in the impinging jet system, initial attachment fluxes under favorable conditions in the packed column were practically insensitive to flow rate. The initial fluxes under favorable conditions were determined at an ionic strength of 0.001 M. Insensitivity of initial attachment flux to ionic strength under favorable conditions is expected based on simulations using the particle transport model of Yang et al. [31].

Initial attachment flux to glass in the packed column at the low flow rate and 0.02 M ionic strength could not be obtained since filter ripening (increased removal rate with time) occurred in that experiment.

3.4. Comparison of jet and column systems

Initial attachment fluxes in the packed column under unfavorable conditions were consistently higher for the quartz relative to the glass substratum (by a factor of 2–3) (Fig. 7, Table 2). This consistency was not observed in the impinging jet system, where the highest initial attachment flux was higher for either substrate depending on the flow and ionic strength conditions (Fig. 5, Table 1).

Direct comparison of initial attachment fluxes between the impinging jet and packed column (Fig. 8) indicates that initial attachment fluxes were similar in the two systems, despite the expectation that rear stagnation points in the porous

media would result in significantly greater attachment fluxes in the packed column. However, it must be recalled that the substrata used in the packed column versus the impinging jet were derived from different sources. Hence, the surface and shape characteristics of quartz grains or glass beads in the packed column differed from the quartz or glass substrata used in the impinging jet. These differences were mitigated by comparing deposition efficiencies rather than absolute deposition fluxes, since the deposition efficiencies represent deposition fluxes normalized to those observed favorable conditions (in the absence of an energy barrier).

Direct comparison of deposition efficiencies between the impinging jet and packed column (Fig. 9) indicate that higher deposition efficiencies were obtained for the packed column relative to the impinging jet when quartz substrata were used, whereas deposition efficiency was lower for the packed column relative to the impinging jet when glass substrata were used, although in the case of glass substrata there was only one experimental condition common to the two systems (high flow rate, 0.02 M ionic strength). The higher deposition efficiencies obtained in quartz sand relative to the quartz substratum in the impinging jet are in qualitative agreement with other very recent investigations of bacterial deposition [13,14]. Deposition efficiencies were all unity or less, as expected. No deposition efficiencies were obtained for the packed column at the low flow rate since filter ripening was observed under favorable conditions. Deposition efficiencies

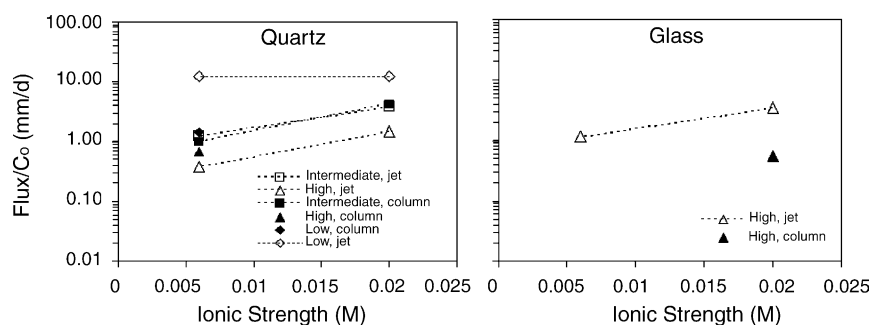


Fig. 8. Initial attachment flux vs. ionic strength and flow rate for 1.1 μm microspheres in the impinging jet (open symbols) and the packed column (closed symbols), with both quartz and glass substrata. Lines do not represent data, but are present only to clarify trends.

decreased with increasing flow rate in the impinging jet and packed column systems for both substrata.

Favorable conditions were generated differently in the impinging jet (PEI-coated quartz) versus the packed column (amine-functionalized microspheres). The similar attachment fluxes obtained under favorable conditions generated by these two different means (compare Figs. 5 and 7) increase confidence in comparison between the jet and column systems despite having generated favorable conditions in these two systems by different means.

3.5. Mixed microspheres in the packed column and impinging jet

Experiments performed in the packed column with a mixture of the 1.1 and 5.7 μm microspheres (Fig. 4) showed that the attachment of the 1.1 μm microspheres was greatly enhanced in the presence of the 5.7 μm microspheres. This is observed from the much lower breakthrough plateau in the presence versus the absence of the 5.7 μm microspheres. In contrast to the column system, the net attachment flux of 1.1 μm microspheres in the impinging jet system was dramatically decreased in the presence of the 5.7 μm microspheres, from 12.2 mm day^{-1} (solo) to 4.53 mm day^{-1} (mixed) (impinging jet data not shown).

4. Discussion

4.1. Hydrodynamic drag

The fact that initial attachment fluxes under unfavorable conditions decreased with increased flow rate in the impinging jet and packed column systems (Figs. 3, 5 and 7) cannot be attributed to greater excluded areas associated with blocking by attached microspheres, since the low attached numbers at this stage of the experiment precluded significant blocking effects. The decreased initial attachment flux with increased flow rate may be due to either: (1) decreased particle flux across streamlines, where cross-streamline flux is driven by settling, diffusion, and interaction forces, or (2) increased hy-

drodynamic drag at the surface. These two processes could potentially be distinguished by the use of the particle transport model to determine the effect of velocity increases on cross-streamline particle flux. The particle transport model predicted negligible deposition flux under unfavorable conditions (as expected), however, the predicted deposition flux increased with increased flow rate under unfavorable conditions. This predicted trend opposes the experimentally observed decrease in attachment flux with increased flow rate under unfavorable conditions, indicating that the model fails to account for effects of hydrodynamic drag under unfavorable conditions. Decreased initial attachment flux with increased flow rate was also observed by Varennes and van de Ven [48] and Meinders et al. [16] and was suggested to be related to hydrodynamic drag. Furthermore, Prieve and Lin [49] demonstrated via simulations that tangential hydrodynamic drag experienced by colloids associated with a surface via the secondary minimum would be expected to yield decreased attachment flux with increased flow rate.

The particle transport model also predicted that attachment flux under favorable conditions would increase with increasing flow rate (Table 1). In contrast, the experimental results under favorable conditions showed little change (no trend) in attachment flux with increased flow rate. This discrepancy also indicates a mitigating effect of hydrodynamic drag on the attachment of microspheres of sizes 1 μm or greater.

Further supporting the notion that hydrodynamic drag mitigates attachment in this system are predictions by the particle transport model (impinging jet simulations) that the 5.7 μm microspheres would undergo a 34.0 mm day^{-1} attachment flux in the impinging jet. Hydrodynamic drag is implicated as an important governor of deposition flux for micron-sized and larger colloids by the lack of attachment of the 5.7 μm microspheres, and the counter-theory trends in attachment flux versus flow rate.

Deposition efficiencies also decreased with increased flow rate (Fig. 9) regardless of system or substratum. Why flow rate should affect this parameter is not clear. The observation indicates that deposition efficiency relates to hydrodynamic forces in addition to interaction forces.

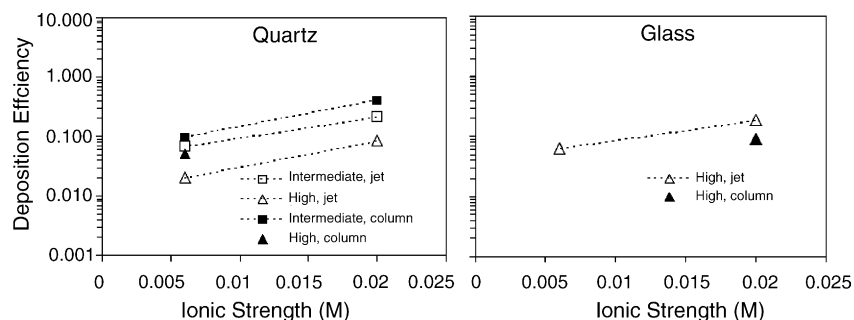


Fig. 9. Deposition efficiencies vs. ionic strength and flow rate for 1.1 μm microspheres in impinging jet (open symbols) and the packed column (closed symbols), with both quartz and glass substrata. Deposition efficiencies were determined by normalizing initial attachment fluxes under unfavorable conditions by those determined under favorable conditions at the corresponding flow rate. Initial attachment fluxes determined under favorable conditions at a particular ionic strength (0.02 M in impinging jet, 0.001 M in packed column) were used in calculations of deposition efficiencies at other ionic strengths, with the expectation that initial attachment fluxes were insensitive to ionic strength under favorable conditions. Lines do not represent data, but are present only to clarify trends.

4.2. Rear stagnation points

For the quartz substratum, greater deposition efficiencies were obtained in the packed column relative to the impinging jet (Fig. 8). Redman et al. [13] and Walker et al. [14] both observed greater bacterial deposition efficiencies in quartz sand relative to a quartz substratum in an impinging jet, in qualitative agreement with our results presented here for the quartz substrata. Those authors attributed this difference to deposition in secondary minima in the quartz sand, which was supported by the elution of a majority of the microspheres from the packed bed upon introduction of pure water to the column. Since colloids associated with secondary minima would be subjected to translation by flow, the authors concluded that the colloids must have accumulated in rear stagnation points within the porous media. In the experiments described in references [13] and [14], ultra-violet absorbance was used for monitoring effluent cell concentrations in the column experiments, whereas plasmid-introduced fluorescence was used for monitoring cell concentrations in the impinging jet experiments. Since different bacterial strains express fluorescence proteins to different extents, the use of different monitoring techniques for the two systems yields the possibility of analytical artifacts. Although we did not examine elution of deposited microspheres in response to introduction of pure water in the experiments shown here, subsequent preliminary results in our laboratory also indicate that the majority of microspheres deposited in the quartz sand are eluted upon introduction of pure water. In contrast, a negligible fraction of microspheres detach from the quartz substratum in the impinging jet upon elution with pure water, further indicating that deposition within the quartz sand was enhanced relative to the impinging jet by deposition “within” the secondary energy minimum.

In contrast to the quartz substratum, the deposition flux in the glass bead packed column was lower than that on the glass substratum in the impinging jet (Fig. 9). This result may suggest that the smooth and spherical nature of the glass beads did not provide rear stagnation points for enhanced colloid accumulation in the glass bead porous

media. However, additional experiments beyond the single condition examined here are needed to further assess this possibility.

4.3. Mixed microspheres

Experiments run in the column with a mixture of the 1.1 and 5.7 μm microspheres (Fig. 4) showed that the attachment of the 1.1 μm microspheres was greatly enhanced in the presence of the 5.7 μm microspheres, indicating that there was either direct or indirect association of these microspheres during attachment. Indirect association might occur in the form of “hiding” of the 1.1 μm microspheres within hydrodynamic shadows formed by attached 5.7 μm microspheres. Although initial deposition would not be expected to occur within a hydrodynamic shadow, colloid rolling following initial deposition may concentrate colloids on the leeward sides of attached colloids. The result would be indirect association of colloids with upstream colloids by virtue of their residence within the hydrodynamic shadow of the upstream colloid.

An additional 1.2×10^9 1.1 μm microspheres were attached in the porous media due to the presence of the 5.7 μm microspheres, based on 60% versus 95% removal in the absence versus presence of the large microspheres (Fig. 4). Given that approximately 1.5×10^8 5.7 μm microspheres were attached (60% attachment) under both solo and mixed conditions; there would have been an average of eight 1.1 μm microspheres associated with each attached 5.7 μm microsphere, assuming direct association between the two. If the association was direct, it would be reasonable to expect it to have affected the transport of the large microspheres. Instead, the transport of the 5.7 μm microspheres was unaffected by the presence of the 1.1 μm microspheres (Fig. 10). Furthermore, flow cytometry counts of the 1.1 μm microspheres in influent samples (0.02 M) should have shown decreases in the order of 40% due to direct association of 1.1 and 5.7 μm microspheres, and a significant fraction of the 5.7 μm microsphere counts should have been converted to “dual positives” (signals from combined microspheres). Instead, counts of

1.1 μm microspheres were unchanged, and a negligible fraction of 5.7 μm microsphere counts were converted to dual positive counts (<3%).

The above analysis indicated that the retained 1.1 μm microspheres were indirectly associated with retained 5.7 μm microspheres in the packed column. A strongly contrasting result was obtained in the impinging jet system, where the initial attachment flux of 1.1 μm microspheres was dramatically decreased in the presence of the 5.7 μm microspheres. No attachment of 5.7 μm microspheres was, in fact, observed under the impinging jet under solo or mixed conditions. Movement of the observation area away from the jet to regions of lower velocity (and consequently lower hydrodynamic drag) revealed attachment of the 5.7 μm microspheres, with increasing surface density of the 5.7 μm microspheres with increasing distance from the jet. Qualitative observations were also made using a parallel plate flow cell since it offered a greater penetration depth of the evanescent field, making visible the mobile 5.7 μm microspheres proximal to the surface. The 5.7 μm microspheres appeared to carry 1.1 μm microspheres, based on their projected images. The apparent direct association of 1.1 μm microspheres with 5.7 μm microspheres in the impinging jet indicates that direct association likely also governed the enhanced attachment of the 1.1 μm microspheres in the presence of the 5.7 μm microspheres in the column system.

4.4. Possible effects of roughness of the quartz substrata in the impinging jet

The initial attachment flux to quartz in the impinging jet showed no sensitivity to ionic strength at the 0.01 ml min^{-1} flow rate. Fig. 5 also shows that the initial flux in the impinging jet was more sensitive to flow rate on quartz substrata than on glass substrata. An electrostatic barrier to deposition

on quartz existed, since its effect manifested at the 0.03 and 0.05 ml min^{-1} flow rates (Fig. 5). However, it seems that an attribute of the quartz (possibly physical) produced a lack of sensitivity to ionic strength at the 0.01 ml min^{-1} flow rate. Based on the fact that the attachment flux to quartz increased greatly as flow rate decreased, to an extent much greater than glass, it is hypothesized that surface roughness of the quartz provided a physical means of enhancing attachment and overriding the effects of ionic strength at the low flow rate.

Initial attachment fluxes in the packed column under unfavorable conditions were consistently higher for the quartz relative to the glass substratum (by a factor of 2–3) (Fig. 7, Table 2), also suggesting an attachment-enhancing effect of roughness in the quartz, consistent with the observations of others (e.g. Refs. [7,9]).

5. Conclusions

Impinging jet experiments indicated a mitigating role of hydrodynamic drag on colloid attachment for μm -sized colloids. This was indicated by the observation that deposition flux under unfavorable conditions decreased with increasing flow rate, and deposition flux under favorable conditions did not increase with flow rate, contrary to predictions by a particle transport model that accounted for the effects of flow rate on cross-streamline flux due to diffusion, settling, and interaction forces. Also signaling a mitigating effect of hydrodynamic drag on particle deposition was the fact that the particle transport model predicted significant attachment fluxes for 5.7 μm sized colloids under unfavorable conditions, whereas no attachment of these colloids was observed in the impinging jet.

Deposition efficiencies in the packed column were significantly higher than those in the impinging jet under the same conditions when a quartz substratum was examined. In contrast, for a glass substratum, deposition efficiency was lower for the packed column relative to the impinging jet under the one condition examined. These results indicate that angular and rough porous media grains (typical of quartz sand) yield enhanced deposition in the column relative to the impinging jet, possibly by colloid deposition in rear stagnation points.

Acknowledgements

This work was funded by grants to William P. Johnson from the National Science Foundation Hydrologic Sciences Program (EAR 0087522), and the National Science Foundation Office of International Science and Engineering (INT-0239482). Any opinions, findings, conclusions or recommendations expressed in this material are those of the authors, and do not necessarily reflect the views of the National Science Foundation.

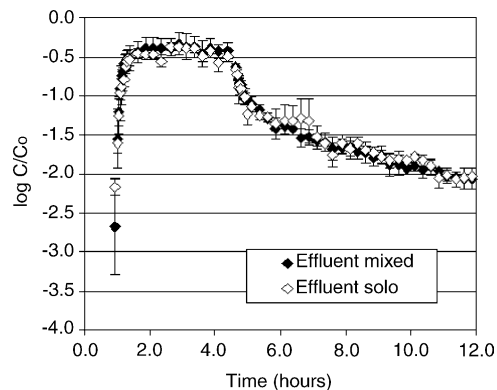


Fig. 10. Breakthrough–elution curve for the 5.7 μm microspheres in packed column experiments in the presence (mixed, closed symbols) and absence (solo, open symbols) of 1.1 μm microspheres at velocity = 4 m day^{-1} and ionic strength = 0.02 M. C_0 and C represent the injected and effluent concentrations, respectively. The duration of the particle injection was ≈ 3.3 h and was followed by ≈ 8 h of elution with particle-free solution. Error bars represent standard deviations in results from replicate experiments ($n = 3$ –4).

References

- [1] J.A. Davis, *Geochim. Cosmochim. Acta* 46 (1982) 2381–2393.
- [2] E.A.D.C. Tipping, *Geochim. Cosmochim. Acta* 46 (1982) 75–80.
- [3] M. Elimelech, C.R. O'Melia, *Langmuir* 6 (6) (1990) 1153–1163.
- [4] J.E. Tobiasson, C.R. O'Melia, *J. Am. Wat. Works Assoc.* 80 (12) (1988) 54.
- [5] T. Dabros, T.G.M. van de Ven, *Colloid Polym. Sci.* 261 (1983) 694–707.
- [6] D.C. Prieve, S.G. Bike, N.A. Frej, *Faraday Discuss. Chem. Soc.* 90 (1991) 209.
- [7] M. Elimelech, C.R. O'Melia, *Environ. Sci. Technol.* 24 (1990) 1528–1536.
- [8] L. Song, P.R. Johnson, M. Elimelech, *Environ. Sci. Technol.* 28 (1994) 1164–1171.
- [9] K. Shellenberger, B.E. Logan, *Environ. Sci. Technol.* 36 (2002) 184–189.
- [10] D. Grasso, K. Subramaniam, M. Butkus, K. Strevett, J. Bergendahl, *Rev. Environ. Sci. Biotechnol.* 1 (2002) 17–38.
- [11] B.A. Jucker, A.J.B. Zehnder, H. Harms, *Environ. Sci. Technol.* 39 (1998) 2909–2915.
- [12] T.R. Neu, *Microb. Rev.* 60 (1996) 151.
- [13] J.A. Redman, S.L. Walker, M. Elimelech, *Environ. Sci. Technol.* 38 (6) (2004) 1777–1785.
- [14] S.L. Walker, J.A. Redman, M. Elimelech, *Langmuir* 20 (18) (2004) 7736–7746.
- [15] J.M. Meinders, J. Noordmans, H.J. Busscher, *J. Colloid Interface Sci.* 152 (1992) 265–280.
- [16] J.M. Meinders, H.J. Busscher, *Colloid Polym. Sci.* 272 (1994) 479–486.
- [17] J.M. Meinders, H.C. Van der Mei, H.J. Busscher, *J. Colloid Interface Sci.* 176 (1995) 329–341.
- [18] L. Song, M. Elimelech, *Colloid Surf. A: Phys. Eng. Asp.* 73 (1993) 49–63.
- [19] L. Song, M. Elimelech, *J. Colloid Interface Sci.* 167 (1994) 301–313.
- [20] P.R. Johnson, N. Sun, M. Elimelech, *Environ. Sci. Technol.* 30 (11) (1996) 3284–3293.
- [21] C. Ko, M. Elimelech, *Environ. Sci. Technol.* 34 (2000) 3681–3689.
- [22] J.M. Meinders, H.J. Busscher, *Langmuir* 11 (1995) 327–333.
- [23] H.H.M. Rinjaarts, W. Norde, E.J. Lyklema, A.J.B. Zehnder, *Environ. Sci. Technol.* 30 (10) (1996) 2869–2876.
- [24] T. Dabros, T.G.M. van de Ven, *Colloid Surf. A: Phys. Eng. Asp.* 75 (1993) 95–104.
- [25] Z. Adamczyk, B. Siwek, L. Szyk, *J. Colloid Interface Sci.* 174 (1995) 130–141.
- [26] T. Dabros, T.G.M. van de Ven, *Int. J. Multiphase Flow* 18 (5) (1992) 751–764.
- [27] T. Dabros, *Colloid Surf.* 39 (1989) 127–141.
- [28] T. Dabros, T.G.M. van de Ven, *J. Colloid Interface Sci.* 149 (2) (1992) 493–505.
- [29] D. Axelrod, *Meth. Cell Biol.* 30 (1989) 245–270.
- [30] Y. Lüthi, J. Rička, *J. Colloid Interface Sci.* 206 (1998) 302–313.
- [31] C. Yang, T. Dabros, D. Li, J. Czarnecki, J. Masliyah, *J. Colloid Interface Science* 208 (1998) 226–240.
- [32] R. Hogg, T.W. Healy, D.W. Fuerstenau, *Trans. Faraday Soc.* 62 (1966) 1638.
- [33] Israelachvili, J.N., *Intermolecular and Surface Forces*, 2nd ed., 1992, Academic Press, London.
- [34] L. Bergstrom, *Adv. Colloid Interface Sci.* 70 (1997) 125–169.
- [35] J. Bergendahl, D. Grasso, *AIChE J.* 45 (3) (1999) 475–484.
- [36] M.V. Smoluchowski, *Z. Phys. Chem.* 92 (1918) 129–168.
- [37] H. Oshima, *J. Colloid Interface Sci.* (1994) 474–483.
- [38] H. Oshima, *Colloid Surf. A: Physicochem. Eng. Asp.* (1995).
- [39] H. Morisaki, S. Nagai, H. Ohshima, E. Ikemoto, K. Kogoe, *Microbiology* 145 (1999) 2797–2802.
- [40] H. Hayashi, S. Tsuneda, A. Hirata, H. Sasaki, *Colloid Surf. B: Biointerf.* 22 (2001) 149–157.
- [41] M. Elimelech, M. Nagai, C.H. Ko, J.N. Ryan, *Environ. Sci. Technol.* 34 (11) (2000) 2143–2148.
- [42] X. Li, T.D. Scheibe, W.P. Johnson, *Environ. Sci. Technol.* 38 (2004) 5616–5625.
- [43] T.D. Scheibe, B.D. Wood, *Water Resour. Res.* 39 (4) (2003) 1080.
- [44] J. Bergendahl, D. Grasso, *Chem. Eng. Sci.* 55 (2000) 1523–1532.
- [45] S.K. Chan, K.M. Ng, *Powder Technol.* 54 (1988) 147–155.
- [46] A.C. Payatakes, C. Tien, R.M. Turian, *AIChE J.* 19 (1973) 58–66.
- [47] Y.J.R.A.M.B. Luthi, *J. Colloid Interface Sci.* 206 (1998) 314–321.
- [48] S. Varennes, T.G.M. van de Ven, *Physicochem. Hydrodyn.* 9 (3–4) (1987) 537–559.
- [49] D.C. Prieve, M.M.J. Lin, *J. Colloid Interface Sci.* 76 (1) (1980) 32–47.